

R85-956642

Investigation of Breadboard Temperature
Profiling System for SSME Fuel Preburner
Diagnostics

Final Technical Report
Contract NAS8-34655

J. A. Shirley

January 1986

Prepared for
George C. Marshall Space Flight Center
Marshall Space Flight Center, Alabama 35812

United Technologies Research Center
East Hartford, Connecticut 06108

R85-956642

Investigation of Breadboard Temperature
Profiling System for SSME Fuel Preburner
Diagnostics

TABLE OF CONTENTS

	<u>Page</u>
SUMMARY	1
INTRODUCTION	2
FIBER OPTIC RAMAN THERMOMETRY	4
Optical Fiber Tests	4
Optical Head Tests	10
Simulated Raman Measurements	15
Comparison to Predicted Signal Rates	28
Discussion of Results	33
CONCLUSIONS AND RECOMMENDATIONS	38
REFERENCES	39

R85-956642

Investigation of Breadboard Temperature Profiling System
for SSME Fuel Preburner Diagnostics

SUMMARY

Results of an experimental investigation performed by United Technologies Research Center (UTRC) under Contract NAS8-34655, sponsored by the George C. Marshall Space Flight Center to determine the feasibility of temperature profiling in the space shuttle main engine (SSME) fuel preburner are presented. In this application it is desired to measure temperature in the preburner combustor with a remote, non-intrusive optical technique. A previously reported conceptual design study identified a system using spontaneous Raman backscattering excited by a remotely-located argon ion laser propagated to the SSME through a small diameter optical fiber as the best approach. The results of measurements with a breadboard Raman system are described in this report. The hot, high pressure atmosphere of the SSME fuel preburner is simulated by a static, electrically heated high pressure optical cell containing molecular hydrogen. Experiments have included: tests of multimode optical fibers for transmission of argon ion laser radiation at 488 nm; tests of a breadboard version of the optical head used to couple the laser probe into the combustor and collect backscattered Raman-shifted radiation; and Raman tests of the entire system with the high pressure cell. Initial measurements, observing Raman scattering from pure rotational transitions were not completely successful, because of interferences from stimulated Raman radiation generated by the high power laser radiation in the optical fiber which is subsequently Rayleigh scattered in the test cell. Measurements of vibrational Raman scattering were successful, and the results of experiments undertaken up to temperatures of 1100 K and pressures to 4500 psia are reported. Temperature precision and accuracies down to 3 percent have been demonstrated with good spatial resolution ($< .04 \text{ cm}^3$).

INTRODUCTION

There is no capability at present to measure gas temperatures in the hot gas path of the space shuttle main engine (SSME), except by the insertion of thermocouples through existing access ports. Thermocouples may perturb the flow yielding inaccurate results and furthermore are generally slow to respond. Future engine developments and improvements to the present engine will most likely require accurate means to measure hot gas temperatures in critical SSME system components with high spatial and temporal resolution. The objective of this investigation is to develop a nonperturbing optical diagnostic technique for measuring gas temperature profiles in the SSME fuel preburner. This report describes the results of a successful experimental investigation of breadboard hardware for SSME thermometry.

A previous report (Ref. 1) presented the conclusions of a conceptual design study aimed at the development of a nonintrusive, optical means of temperature measurement in the SSME fuel preburner. In that study spontaneous Raman backscattering measurements of hot molecular hydrogen spectra, implemented through optical fibers, was selected as the best technical approach. Key to the selection of this approach was the limited optical access in the existing SSME preburner. Only two transducer ports are available on the existing engine and they are not diametrically opposed. For this reason a single port technique is favored. Spontaneous Raman can be used with this type of access. Furthermore at the extremely high pressures and moderate temperatures existing in the SSME, Raman measurements should be realizable using an optical fiber to convey the laser radiation to the preburner to excite the Raman spectrum, and a second fiber to collect the Raman-shifted radiation and transport it to spectroscopic detection apparatus. The laser and detection apparatus can thereby be located remotely in a protected environment. At the same time the optical fiber provides a relatively protected means of transporting radiation to and from the engine.

In the breadboard hardware development investigations, reported herein, Raman scattering has been measured using optical fibers and a medium power argon-ion laser. An electrically-heated, high pressure optical cell has been used to simulate the high pressure molecular hydrogen conditions existing in the SSME fuel preburner.

The application of moderate power argon-ion (approximately 3-10 Watts) radiation through multimode core fibers has been experimentally investigated. A breadboard version of the optics to focus the laser into the probe volume, to collect Raman scattered radiation and to focus it into another fiber, has been developed. A spatial resolution of 10 mm at working distances up to 270

mm has been demonstrated. The experiments to be described include measurements of Raman scattering from pure rotational transitions, and Q-branch transitions. Rotational scattering measurements were attempted first because calculations predict higher intensities for rotational transitions as opposed to vibrational-rotational transitions. Interferences from stimulated Raman scattering generated in the laser transmitting fiber and from grating scattering, however, were found to preclude such measurements. Vibrational Q-branch measurements overcame both of these limitations. Molecular hydrogen gas temperatures in a heated optical cell were successfully measured. The measurements show, however, that power losses are more severe than anticipated in the transmitter fiber for low order spatial propagation modes in the fiber. Low order modes are needed to obtain good measurement spatial resolution and to couple the collected Raman signal efficiently into the receiver fiber leading to the detection apparatus. This likely means that the laser will need to be located near the preburner (less than 10 meters) to limit power losses. The detection apparatus can still be located remotely, say 40 meters away, from the rocket engine. These measurements indicate that it should be feasible to measure temperatures at about 5 percent precision, with spatial resolution of 1 cm and 10 millisecond temporal resolution.

In the next section of this report the details of the measurement technique are very briefly reviewed. The results of fiber transmission tests are then described, followed by a description of tests of the optical head which couples laser radiation into the preburner and collects Raman backscattered radiation. The results of measurements in the high pressure optical cell are presented next. These results are compared to the predicted performance needed to meet overall measurement goals. Conclusions and recommendations for future investigations are described. References are contained in the last section.

FIBER OPTIC RAMAN THERMOMETRY

This section describes experiments undertaken to develop fiber optic Raman diagnostics for thermometry of the fuel preburner of the space shuttle main engine. The results should be generally applicable where gas densities are high and molecular hydrogen is a dominant species.

The principles upon which Raman thermometry are based are described in the conceptual design report (Ref. 1) prepared under the previous study contract. Reference should be made to that report for the theoretical background for fiber optic Raman thermometry (FORT). The general concept of FORT diagnostics is illustrated in Fig. 1. The system is conceived as composed of a high power continuous wave laser, an optical head mounted directly to the preburner, and a spectrograph/optical multichannel detector (OMD) combination. Optical fibers permit the location of the laser and the detection apparatus at a safe distance from the engine. The optical head serves to focus the laser light into the preburner, defines the probe volume, and collects the Raman-shifted light which is backscattered and focuses it into the receiver fiber. This fiber connects to the spectrograph where the radiation is dispersed and then detected with a multichannel detector. It is the distribution of radiation in the Raman spectrum which determines the gas temperature, as described in Reference 1.

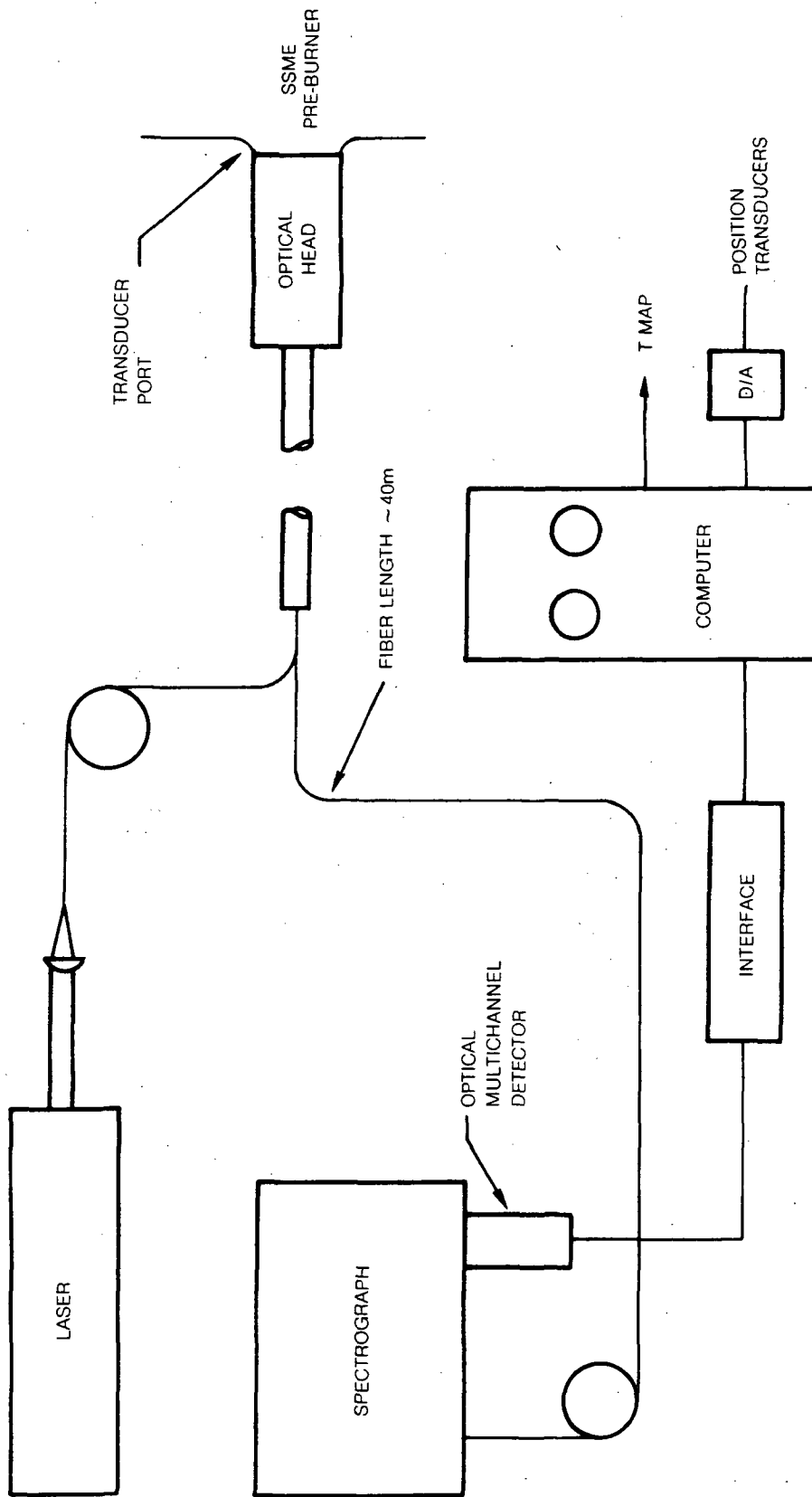
This section begins with a description of tests of the power handling capabilities of commercial optical fibers. Relatively high power radiation is required to be incident on the probe volume to achieve the measurement objectives. Following that discussion is a description of tests to determine the spatial resolution of the optical head. This is an important parameter of the diagnostic system and also is important to characterize in a backscattering system working with a small aperture. After that Raman measurements with the breadboard FORT system are described. In these measurements, conditions in the preburner are simulated by a high pressure, electrically-heated optical cell. Measurements of both pure rotational Raman scattering and vibrational-rotational Q-branch scattering are reported.

Optical Fiber Tests

The transmitter fiber is one of the most critical elements in the FORT diagnostic system. This fiber must transmit the laser radiation without unacceptable attenuation and must not severely degrade the laser beam quality.

The importance of the power handling capability of the transmitter optical fiber was pointed out in the conceptual design report (Ref. 1). There the development followed the analysis of Smith (Ref. 2), who studied the theoretic-

RAMAN DIAGNOSTICS SYSTEM



cal power handling capacity of single mode fibers. He found that stimulated Raman and stimulated Brillouin scattering limit the practical power capacity of small core, low-loss fibers at high radiation intensities. Following Smith's analysis, the critical radiation intensity for laser wavelengths of interest, was estimated in Reference 1 to be approximately 40 kW/cm^2 per transverse mode in the fiber. The critical intensity is the intensity at which nonlinear conversion becomes important, i.e. comparable to the transmitted power. Tests were therefore undertaken to verify these predictions as applied to multimode fibers with core diameters of 50 to 100 microns.

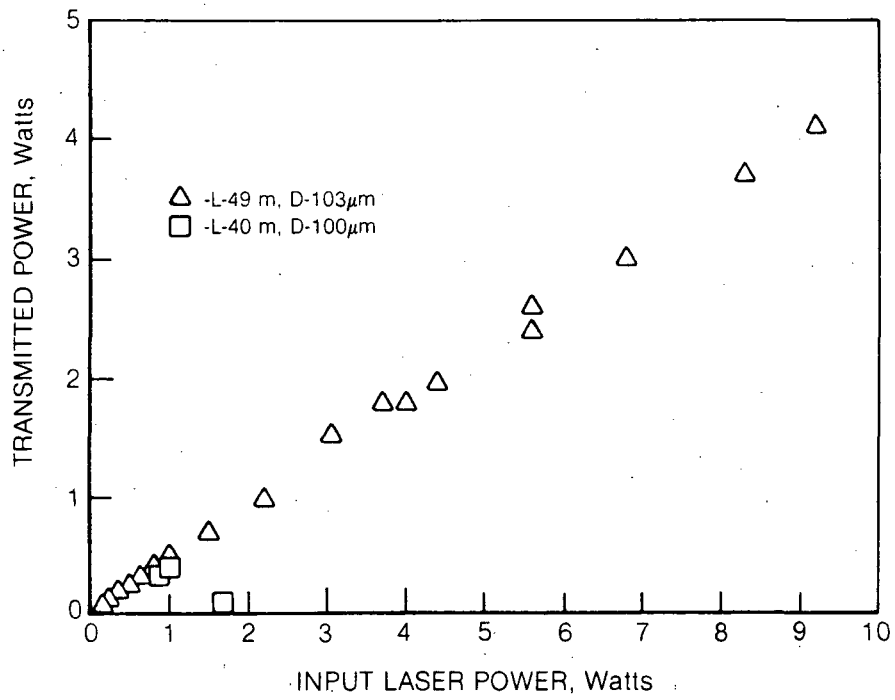
Optical fibers possess excellent transmission characteristics in the near infrared region of the spectrum, having attenuations as low as 0.2 dB/km. Raman scattering is stronger for short wavelengths however, so that operation is desired away from the best transmission windows of the fiber. Attenuation in the fiber generally follows an inverse fourth power relation with wavelength because the dominant loss mechanism at visible wavelengths is Rayleigh scattering. According to this scaling, good fiber attenuation factors in the operating range of the argon ion lasers being considered for this application would be on the order of 20 dB/km.

The transmission of several commercially available multimode fibers has been measured. The ends of the fibers used in these tests were cleaved, rather than lapped and polished, to avoid possible problems with polishing materials or epoxy remaining on or near the ends of the fiber. The results for fibers with core diameters near 100 microns and 50 microns are shown in Figs. 2 and 3, respectively. The size of the laser focal spot size on the end of the fiber was found to be important. Focusing the laser too tightly produced excessively high intensities at the end of the fiber, resulting in failure usually by melting of the output end of the fiber. Fiber failures were experienced using lenses with focal lengths less than about 15 mm, for which focal spot diameters are estimated to be less than 10 microns. Typically the transmission through fibers about 40 meters long was around 50 percent. Accounting for Fresnel reflection losses at the ends of the fiber, the lowest fiber attenuation measured was 49 dB/km for fibers with core diameters near 100 microns, and 32 dB/km for fibers near 50 microns. One 50 micron fiber exhibited nonlinear behavior, perhaps due to Brillouin scattering. Evidence of stimulated Raman scattering in the transmitter fiber was found in the Raman measurements and is discussed in the rotational Raman measurements section.

The results of the tests for the transmission of 488 nm argon ion laser radiation measured with a number of commercial multi-mode core optical fibers are summarized in Table 1.

Measurements were made of the focal properties of the radiation exiting the fiber. In these tests, the argon ion laser was focused into the 50 micron

FIBER TRANSMISSION TESTS ARGON-ION LASER (488 nm)



FIBER TRANSMISSION TESTS ARGON-ION LASER (488 nm)

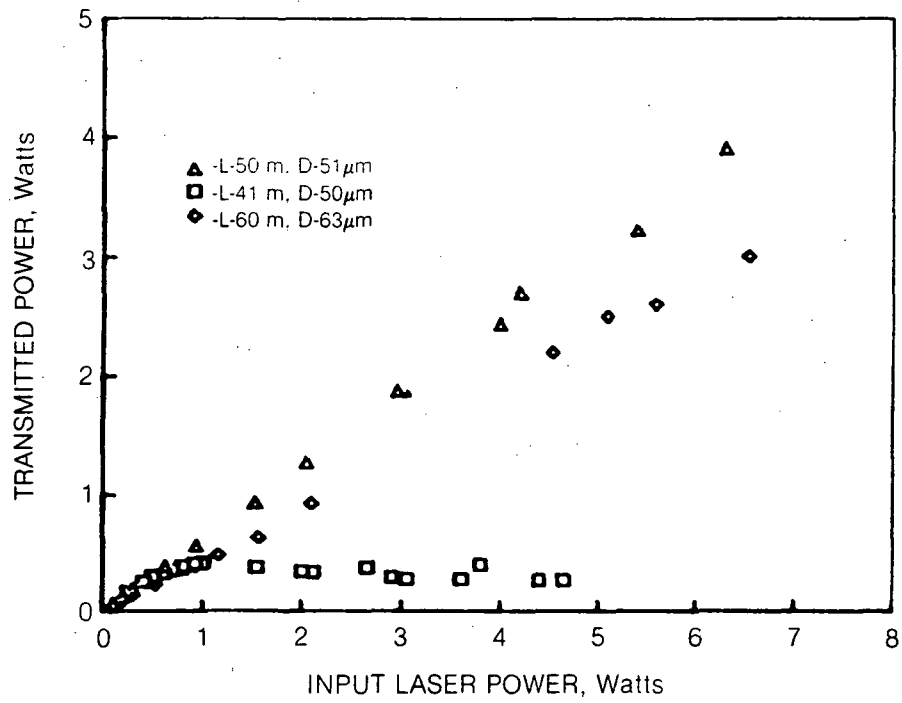


Table 1

Summary of Multi-Mode Fiber Transmission Tests

488 nm Argon-ion Radiation

Fiber	Supplier-No.	Core Dia microns	Clad Dia micron	Length m	Trans.	Atten dB/km	Object- ive	Remarks
001	Newport F-MLD	103	140	50	.44	71	20X	5.2W out
001	Newport F-MLD	103	140	50	.47	52	20X	output fail 8W in
001	Newport F-MLD	103	140	48.5	.50	49	10X	4.2W out
001	Newport F-MLD	103	140	48.5	.44	59	5X	4.1W out
002	Newport F-MSD	51	125	50	.61	32	5X	3.9W out
003	Times Fiber	50	126	41	.61*	39	5X	nonlinear
004	General Fiber	100	140	40	.48	63	5X	nonlinear input fail
005	Corning 1515	63	130	60	.46	45	5X	3 W out

* low power transmission and attenuation, max power out = 0.35 W

fiber with a 25 mm focal length objective and the radiation from the output of the fiber was collimated with a 15 mm objective and focused with a 267 mm focal length plano-convex lens. The resulting beam waist diameter was determined by scanning a knife blade through the beam at the focus (Ref. 3). Power was measured with a thermopile detector located after the knife-blade. The total power of the beam (0.3 W) was kept low to prevent burning the edge of the blade. The waist diameter was determined to be 570 microns. The spot size at the fiber exit face is estimated from the magnification of the lenses to be 32 microns. In tests with a 100 micron core fiber the beam was found to be about 40 microns in diameter at the end of the fiber.

An estimate can be made of the degradation in laser beam quality as a result of propagation through the fiber. The beam at the exit of the laser was measured to be 1.4 times diffraction limited for a TEM_{00} mode. With a beam diameter measured at the end of the fiber of 40 microns, along with a measured divergence of 0.18 radians, the beam is calculated to be 12 times diffraction limited for a TEM_{00} mode. This divergence, which is the full angle, compares with the 0.4 radian full acceptance angle of the fiber. Therefore the beam quality is one-eighth the beam quality of the laser. These estimates are important because they determine how tightly the laser radiation can be focused by the optical head in the measurement volume and therefore affect the measurement spatial resolution.

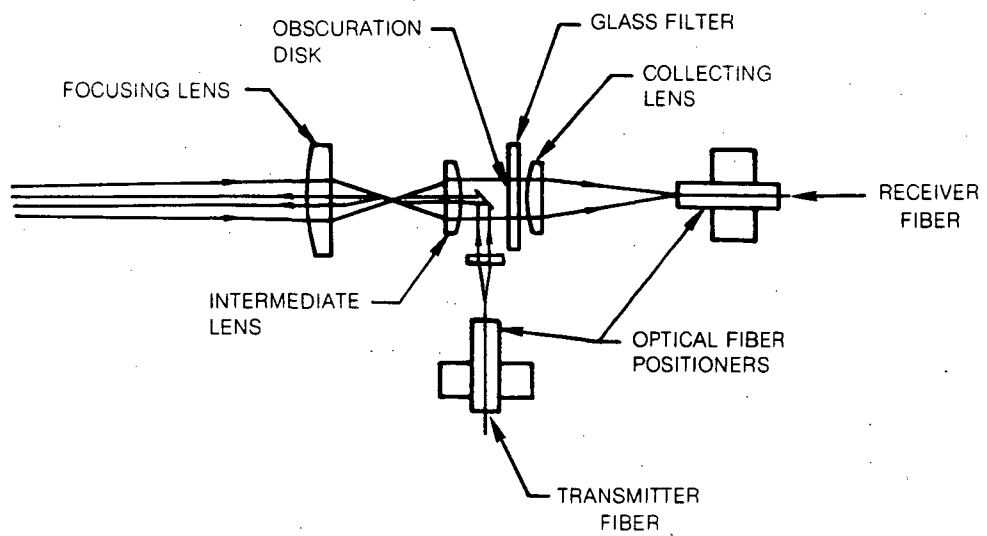
The results of the tests with multimode optical fibers indicate that up to 4 Watts of raw power can be transmitted through the fiber. This is the power level used in signal magnitude estimates in the conceptual design study. Later tests to be described indicate that all of this power is not usable, because it cannot be focused within the collection volume that the receiver fiber views. When focusing into the fiber is adjusted to obtain the smallest focal diameter at the probe volume, the fiber transmission is much lower, approximately 25% or less.

Optical Head Tests

The function of the optical head is twofold. First, the optics must collimate light from the transmitter fiber and focus it at the measurement point in the preburner. Second, the optics must collect backscattered Raman-shifted radiation and focus it into the receiver fiber for transmission to the spectrograph/detector. The design of the optical head determines the measurement volume.

The layout of the optical head design is shown in Fig. 4. The beam from the laser is collimated, and then directed along the principal optical axis of the head by a small prism. An intermediate lens brings the radiation to a

BREADBOARD OPTICAL HEAD DESIGN



real focus and, finally, the focusing lens projects it into the measurement volume (through a high pressure window). The focusing lens collects the backscattered light and focuses it at the intermediate focus. The intermediate lens recollimates the collected light, whence it skims past the prism and is focused onto the receiver fiber. An absorbing glass filter is used to block the unshifted, scattered laser light. By moving either the intermediate lens or the focusing lens along the axis, the focal point of the laser can be changed so that different points across the diameter of the preburner can be probed.

The optical head is forced by constraints of the preburner to operate at large f-numbers when viewing across the combustor. This increases the extent of the measurement volume along the axis, which determines the spatial resolution. It is desired to keep the resolution as small as possible, i.e. 0.5 to 1.0 cm. In a high f-number system, the on-axis rays contribute greatly to the sampling length. If the central rays are blocked, as suggested by Eckbreth and Davis (Ref. 4), the resolution can be improved. The small prism provides some obscuration. Additional obscuration can be provided by an opaque disk centered on the optical axis.

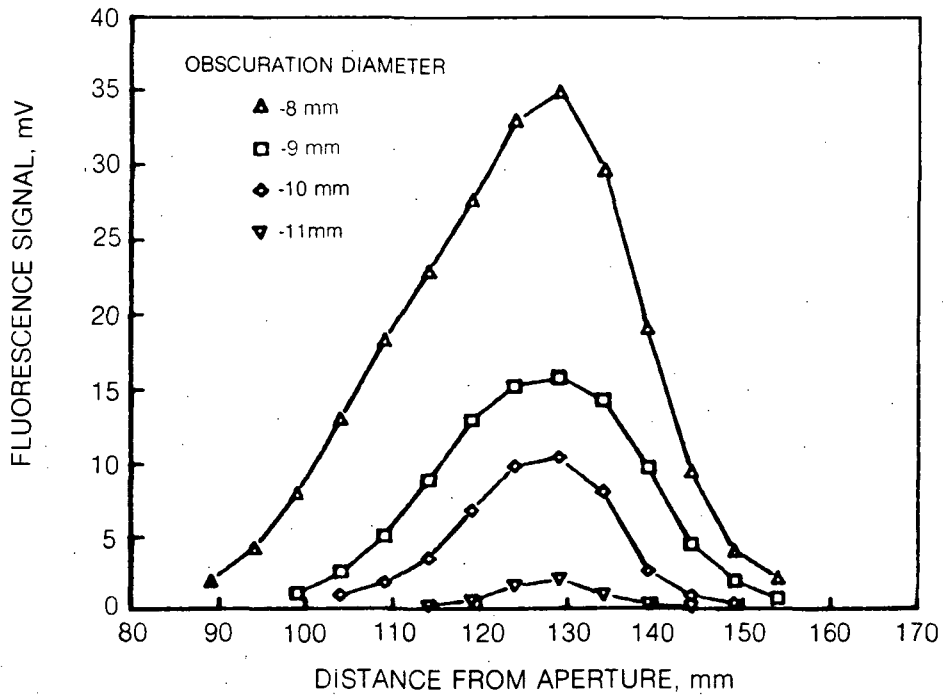
The spatial resolution of the optical head has been measured by simulating Raman scattering in the measurement volume by a thin cell (2 mm) containing a dye that fluoresces in the incident laser light. The cell is translated along the axis to map out the spatial extent of the optical response. For these measurements the laser is chopped and the fluorescence radiation is detected by a photomultiplier tube and phase-sensitive tuned amplifier. Figure 5 shows the results of the measurement of a series of fluorescence profiles. These data show the effect of different obscuration diameters from 8 mm to 11 mm. The maximum obscuration possible depends on the distance at which the system is focused. It is approximately 11.4 mm in this design of the optical head. An appropriately located 1 cm diameter aperture was used to simulate the limiting aperture of the transducer port.

A series of measurements like that shown in Fig. 5 have been carried out to study the effect of observation distance on spatial resolution. The results are shown for one obscuration diameter in Fig. 6. For these tests the distance from the intermediate lens to the final lens is changed to focus at different distances from the limiting aperture. The solid curve shows the spatial resolution calculated from a simple relationship derived in Ref. 4:

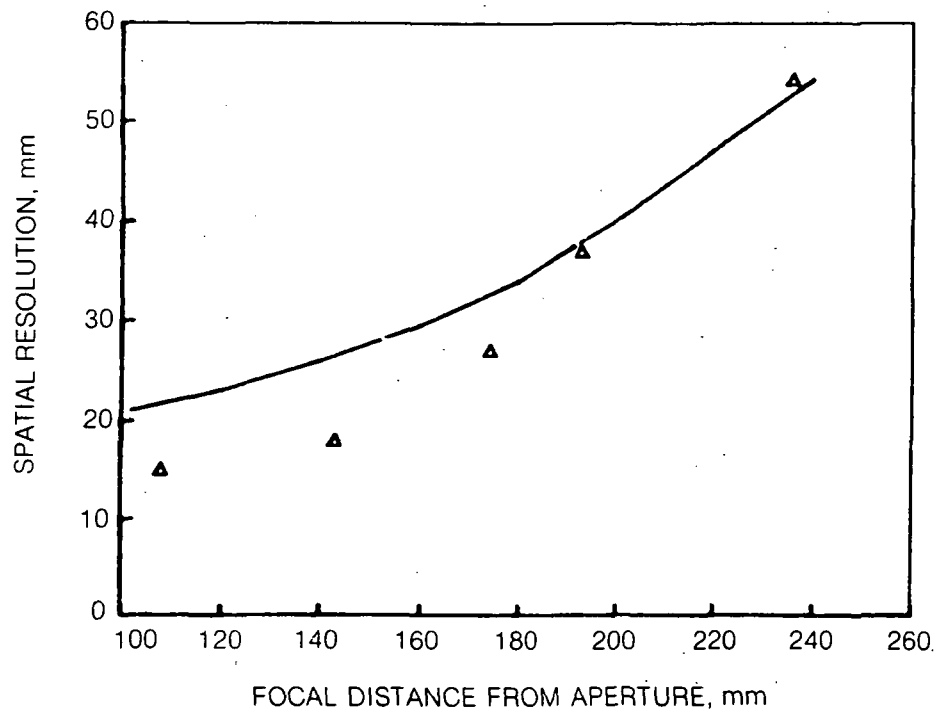
$$\Delta l = \frac{2f(A+B)}{D_0} \quad (1)$$

Here A is the collecting aperture (the receiver fiber core diameter), B is the diameter of the laser spot in the focal volume, f is the distance of the focal

EFFECT OF OBSCURATION ON SCATTERING PROFILE



SUMMARY OF SPATIAL RESOLUTION TESTS
OBSCURATION DIAMETER — 11 mm



point from the focusing lens, and D_o is the diameter of the obscuration disk. The diameter of the laser spot was measured. It can be related to the diameter of the spot at the exit of the transmitter fiber through the magnification of the lenses. Equation (1) is based on simple geometrical concepts within the framework of paraxial ray optics. It should not be expected to give precise results in every case, but is useful for estimating resolution with obscured systems.

The effect of obscuration on the spatial resolution and collected dye signal maximum is shown in Fig. 7. It is clear from this data that the use of larger obscuration diameters to achieve a given spatial resolution incurs a substantial penalty in the collected signal.

It should be pointed out that the optical head used in these tests is a relatively simple design. Simple off-the-shelf plano-convex lenses were used throughout. The design could be improved by the use of lenses optimized to work in this configuration. For example the final lens focusing into the probe volume works at finite conjugates, and a plano convex lens does not give the best results in this case. Furthermore the lens focusing into the receiver fiber functions at an f -number of about 4. This is about the f -number where spherical aberration effects become important. Indeed, in later Raman tests, this particular lens was replaced with a doublet (corrected at the ends of the visible spectrum for chromatic and spherical aberration) and spatial resolutions of 0.5 to 1 cm at a working distance of 275 mm were observed with the 8 mm square obscuration of the laser turning prism. This is nearly an order of magnitude improvement over the results displayed in Fig. 6 and highlights the importance of proper lens design. Thus, with proper lens designs, spatial resolutions of 1 cm are readily achieved with an estimated 66 percent loss in the signal incurred.

An important point is that many of the optical performance parameters, such as spatial resolution and collection efficiency, are determined by how tightly the laser is focused into the probe volume. This is determined largely by the laser beam quality as it exits from the transmitter fiber.

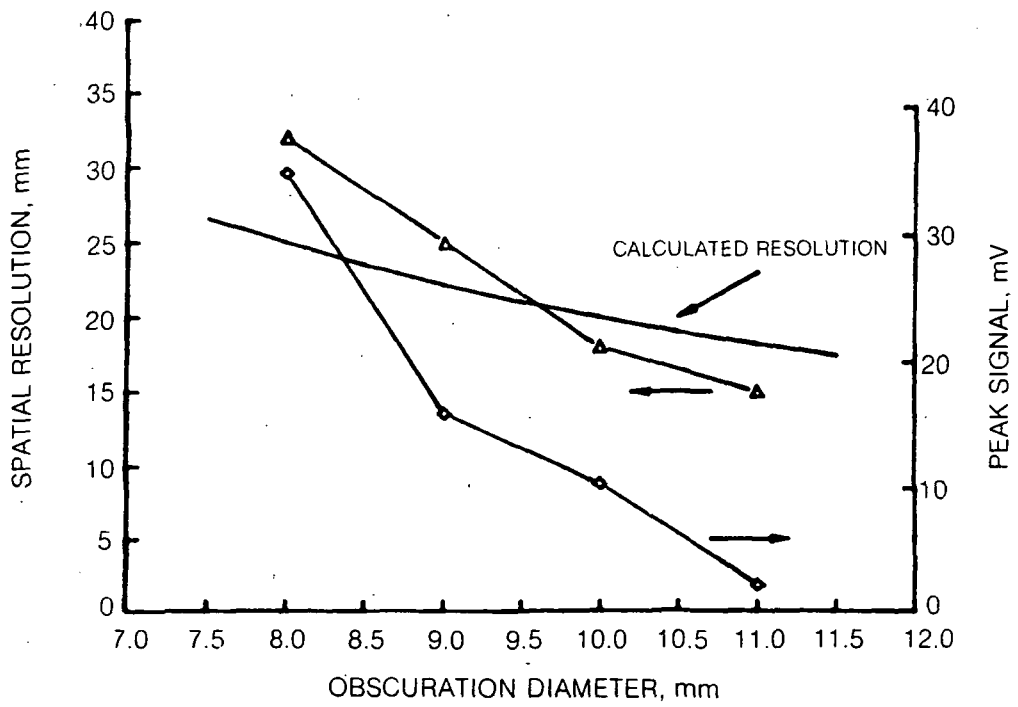
Simulated Raman Measurements

The results of measurements of hydrogen Raman spectra using the fiber system in conjunction with the optical head are described in this section. The results of unsuccessful rotational Raman measurements are described first, followed by a discussion of the successful vibrational Raman measurements.

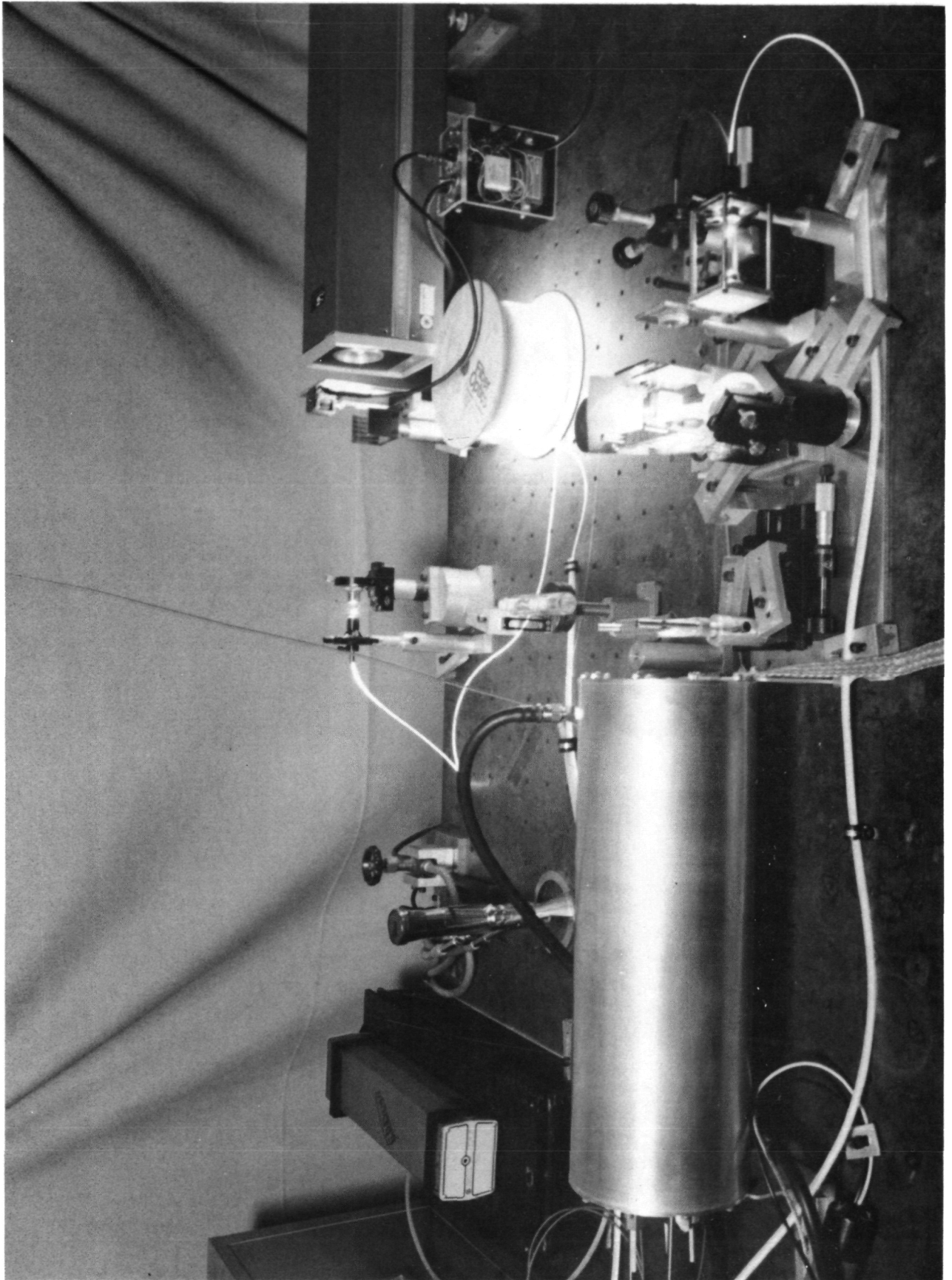
The breadboard FORT diagnostic apparatus is shown in the photograph in Fig. 8. The nominal 3 Watt argon-ion laser is shown to the right in the

EFFECT OF OBSCURATION ON RESOLUTION AND SIGNAL MAXIMUM

WORKING DISTANCE = 85 mm



FORT EXPERIMENTAL APPARATUS



background, focusing into the transmitter fiber. Rayleigh scattering in the transmitter fiber makes it appear to glow. The breadboarded optical head is in the foreground to the right. The large cylinder is the high pressure cell. The receiver fiber can be seen at the optical head, held in the fixture with two micrometer heads, and also at the top center of the photo. The fiber connects to a spectrograph located at the end of the 40 meter fiber in another laboratory. A safety container vessel drops over the cell and optical head for heated, high pressure experiments. The optical head is shown in a close-up photograph in Fig. 9. The intermediate focal point is seen clearly.

Preburner measurements were simulated by heating pure hydrogen in a static high pressure optical cell. Figure 10 shows a cross section through the cell. The cell has 12.7 mm diameter bore, with a central heated region 165 mm long, between windows 335 mm apart. The windows are 25.4 mm thick, 25.4 mm diameter sapphire. Cracking with quartz windows was experienced well below the 6000 psi design pressure. The cell is heated by an internally wound molybdenum heater. The heater is controlled by a set-point temperature controller connected to a thermocouple attached to the center of the heated inner liner.

Sapphire and quartz rods 110 mm long were inserted in the cell with one end of each near the inner surface of the end windows. This was necessary to prevent thermal buoyancy effects from severely bending the optical beam. Without the rods, the Raman signal dropped rapidly with heating of the cell just 50 C above the ambient temperature.

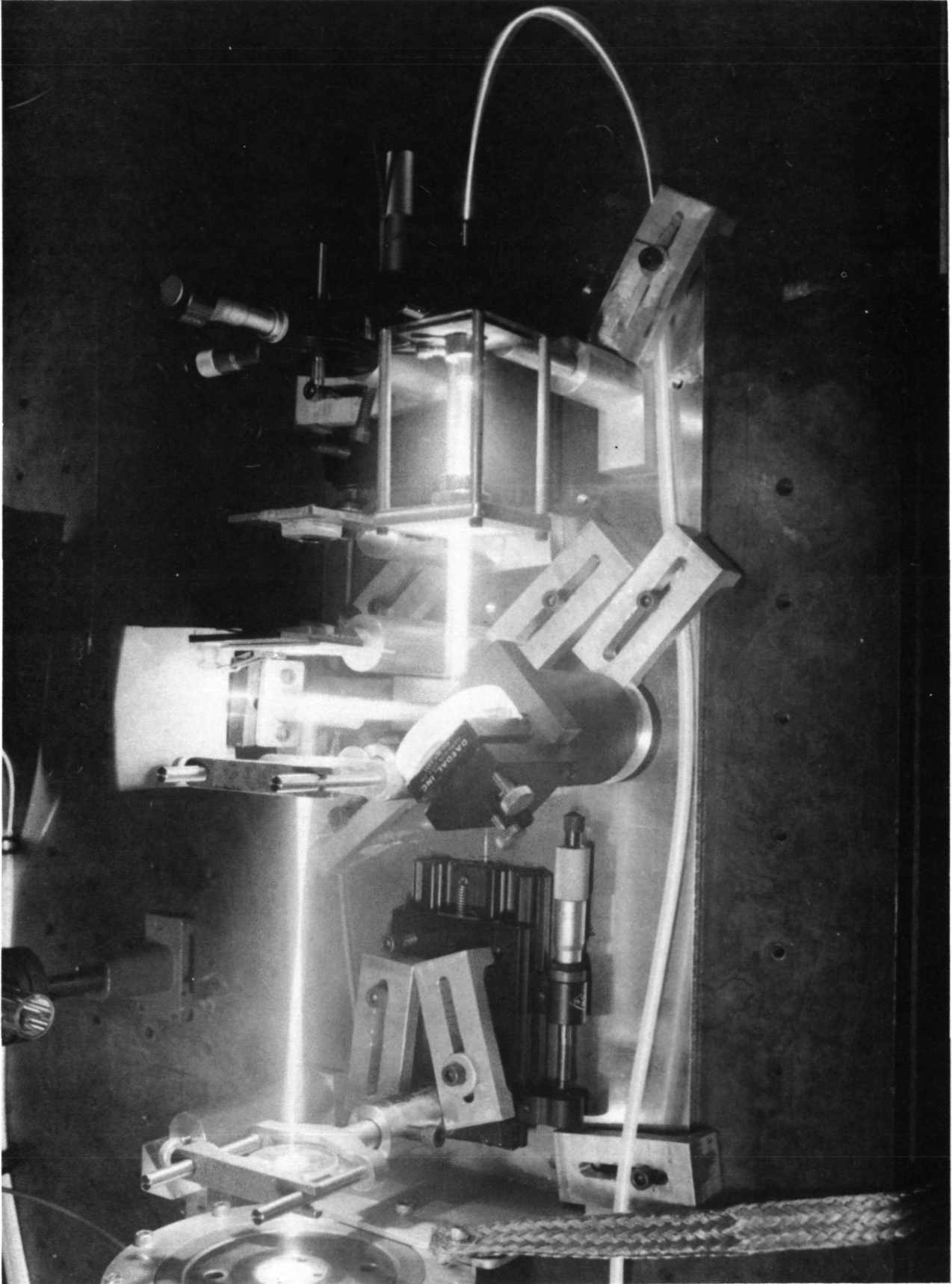
Rotational Raman Measurements

Rotational Raman scattering is calculated to be about 70 percent stronger than vibrational-rotational Raman scattering in the conceptual design report (Ref. 1). Accordingly tests to observe the pure rotational spectrum were undertaken first.

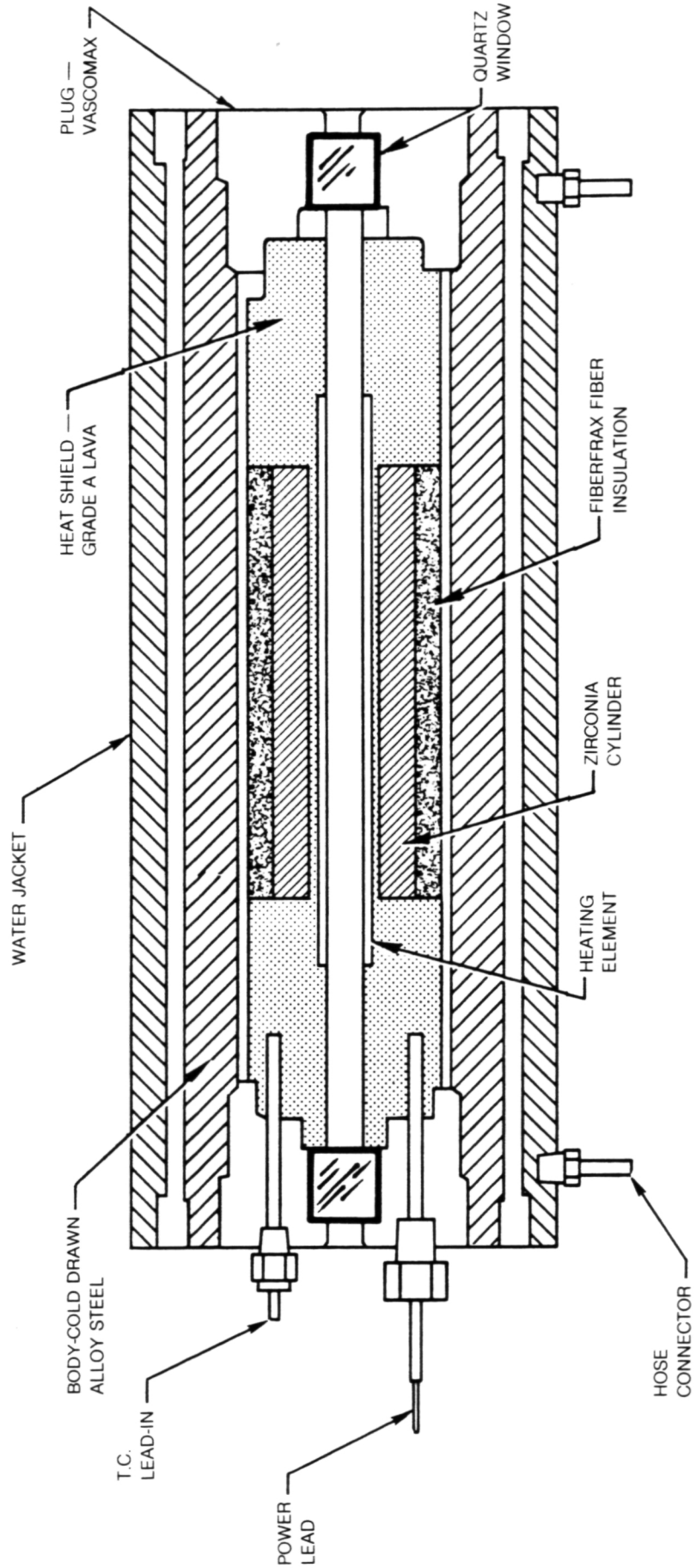
The rotational S-branch of hydrogen was observed from room temperature hydrogen contained in the cell at 1000 psia as shown in Fig. 11. This and other spectra were obtained by measuring the spectrum on an optical multichannel detector with the laser turned on, and subtracting from this spectrum, channel by channel, another spectrum obtained with the laser blocked. The locations of the hydrogen rotational transitions were determined from a wavelength calibration provided by observing the Raman spectrum of liquid toluene placed in a cuvette in the probe volume of the optical system. A broad peak centered at 460 cm^{-1} and a strong background level are present in the rotational Raman spectrum.

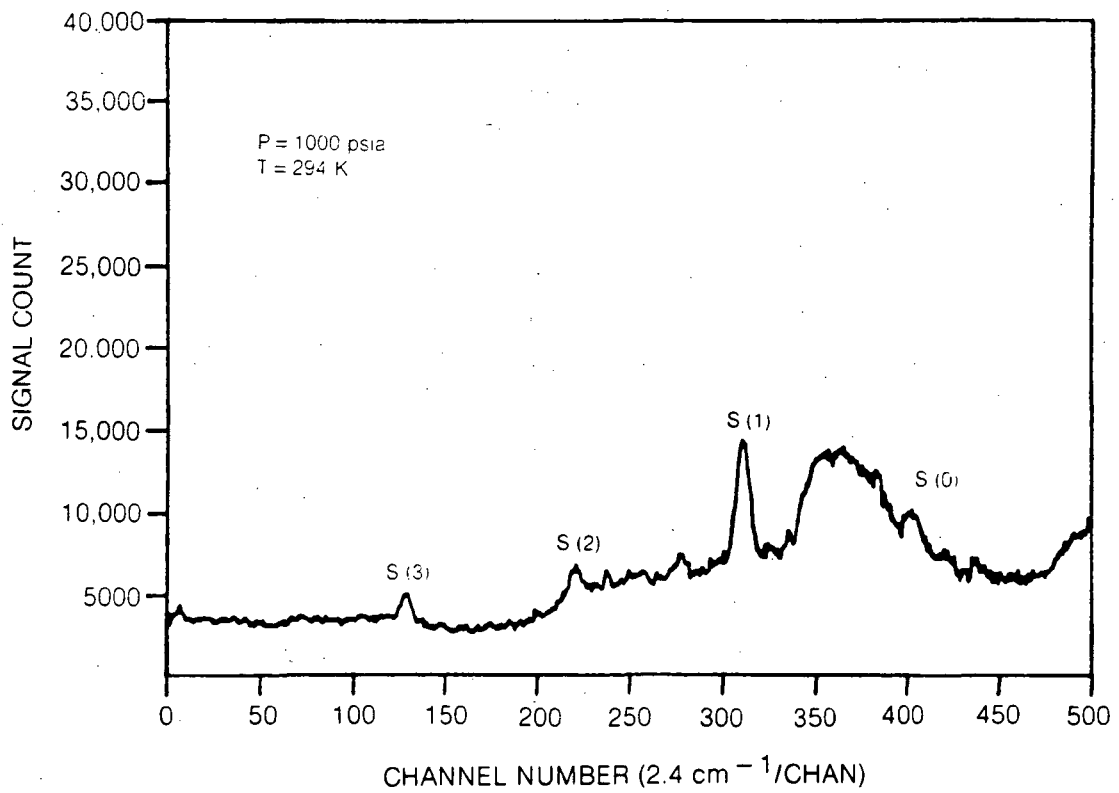
The broad peak is believed to arise from stimulated Raman radiation generated in the transmitter fiber, which is then Rayleigh scattered in the

BREADBOARD FORT OPTICAL HEAD



INTERNALLY HEATED PRESSURE VESSEL FOR RAMAN DIAGNOSTICS



FORT HYDROGEN ROTATIONAL RAMAN SPECTRUM

probe volume of the high pressure cell. The evidence for this assertion is shown in Fig. 12. This figure shows a comparison of two spectra: one using a fiber 40 meters in length to transmit the laser probe radiation and one using a short 1.3 meter fiber. The broad peak nearly disappears in the spectrum with the short fiber. The broad peak was completely absent in tests conducted with no transmitter fiber at all. It should be noted that the Raman shift of the broad peak corresponds closely to the shift reported for SiO_2 -- 467 cm^{-1} (Ref. 5). Comparing the integrated intensity of the broad peak to the hydrogen Raman spectrum and accounting for the Rayleigh scattering cross section of hydrogen (Ref. 6) the stimulated Raman power appears to be about 2 to 3 percent of the 488 nm laser line, assuming all the collected SiO_2 Raman shifted radiation is Rayleigh scattered (there may be some contribution from reflections from optical components).

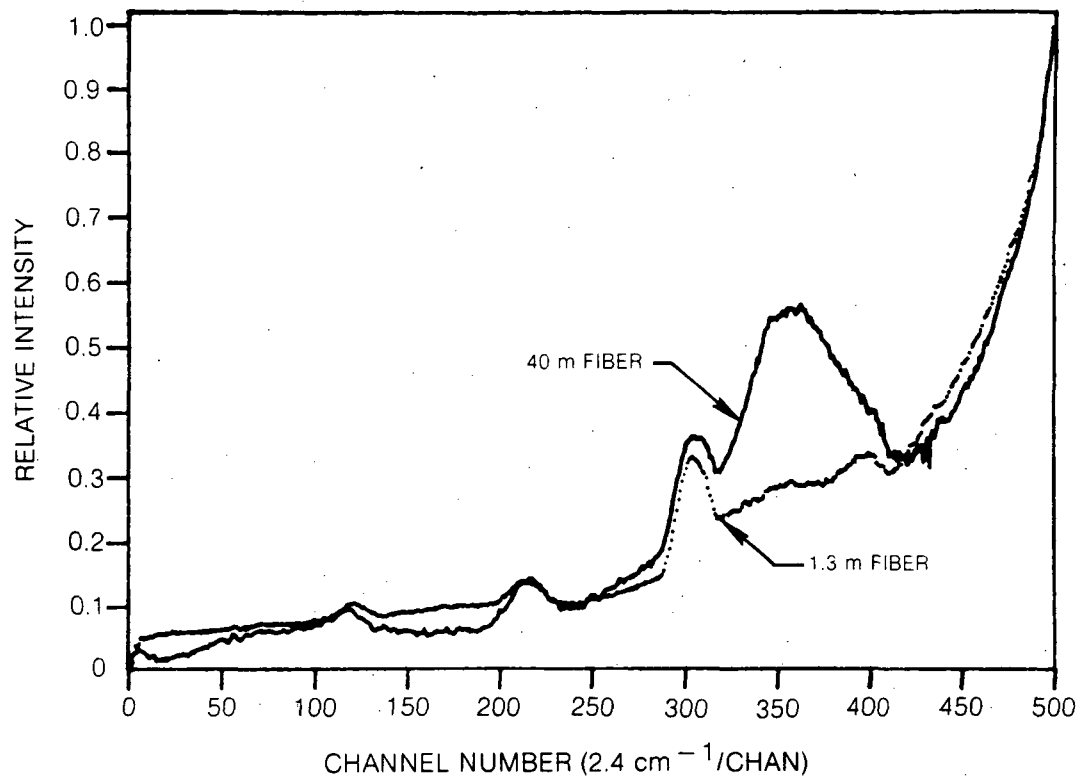
A large background is present in the rotational Raman spectra in Figures 11 and 12. A comparison with a simulated spectrum assuming the background arises solely from Rayleigh scattering shows the background is much too high for this to be the case. The spectrometer was tuned to larger Raman shifts on the Stokes side of the spectrum, that is to longer wavelength where the background steadily dropped to smaller levels. It is believed that the large background is due to grating scatter of the laser radiation in the spectrograph (Ref. 7). Reflections from optical surfaces contribute to the large amount of laser light which enters into the receiver fiber. Except for the collecting lens (see Fig. 4), all the optics in the breadboard optical hardware are uncoated. Anti-reflection coatings would decrease the reflectivity per surface from 4% to less than 0.25%, typically.

There are several strategies for dealing with the spurious broad peak and the large background. The stimulated Raman radiation exiting the transmitter fiber can be blocked with a filter. A short pass dielectric filter was found to be effective, but results in an insertion loss. Using a 90° dispersing prism in the optical path, after the laser radiation from the transmitter fiber is recollimated, was less effective, probably due to the limited dispersion of the prism glass. The only way of effectively dealing with grating scatter is to employ a double spectrograph. A better solution for both problems is to observe vibrational Raman scattering instead.

Vibrational Raman Measurements

The spectrograph used to measure rotational Raman spectra was designed for coupling to a fiber, having an f-number of 2.1. This spectrograph does not focus satisfactorily at the wavelength of H_2 vibrational scattering however and, therefore, could not be used. An available spectrograph with a limited speed (f/6.7) was used. Overfilling by the radiation from the receiver fiber is expected in this instrument.

**EFFECT OF TRANSMITTER FIBER LENGTH ON
SPECTRUM IN ROTATIONAL RAMAN REGION**



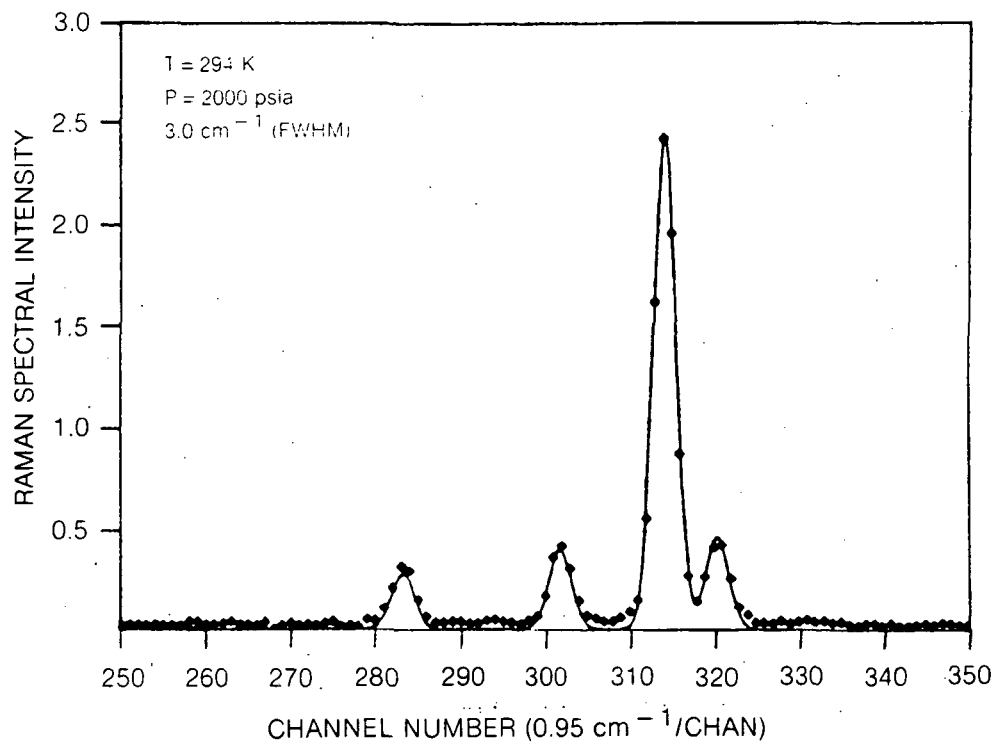
Vibrational Raman spectra from room temperature to 1100 K have been recorded at pressures from 1000 to more than 4000 psia. For heated runs the cell is initially pressurized and sealed off. The pressure rises in this constant volume case, but is not linear with temperature because of the small volume of unheated tubing outside the cell.

Figure 13 shows the measured spectrum of room temperature hydrogen at a pressure of 2000 psia. The points shown as small squares are the measurements, while the calculated spectrum is shown as a solid line. The intensities are calculated from the integrated intensities of Ref. 1 with a Gaussian lineshape model. The rationale for this shape is that the focal intensity distribution refocused after leaving the fiber is usually well approximated by a Gaussian function. The full width at half maximum is determined by comparing calculations at a number of widths to experimental spectra. The calculations show a change in the degree of resolution of the Q(0) and Q(1) lines from which the spectral resolution is determined quite satisfactorily. The agreement with the calculations shown in Fig. 13 is quite good. The only adjustments required, are to scale the calculations to the peak height of Q(1) and to adjust the location of this peak. The spectral dispersion is independently determined from a neon emission lamp spectrum. To obtain a spectrum, the optical multichannel detector is scanned for a set number of frames continuously reading the tube and accumulating the signal with the laser blocked; this procedure samples "dark" current and the natural background radiation. This spectrum is saved and the tube is reread for the same number of frames with the laser unblocked. The dark spectrum then is subtracted from the laser induced spectrum. Typically the dark count rate is 1000 signal counts per second. The baseline signal level far away from the Q-branch lines is 16 counts per second. The standard deviation of this baseline signal is about 3 counts per second. Therefore the baseline probably is mostly due to residual grating scatter of the laser line rather than imperfect background subtraction. Again, anti-reflection coating all the elements in the optical head should substantially reduce this background.

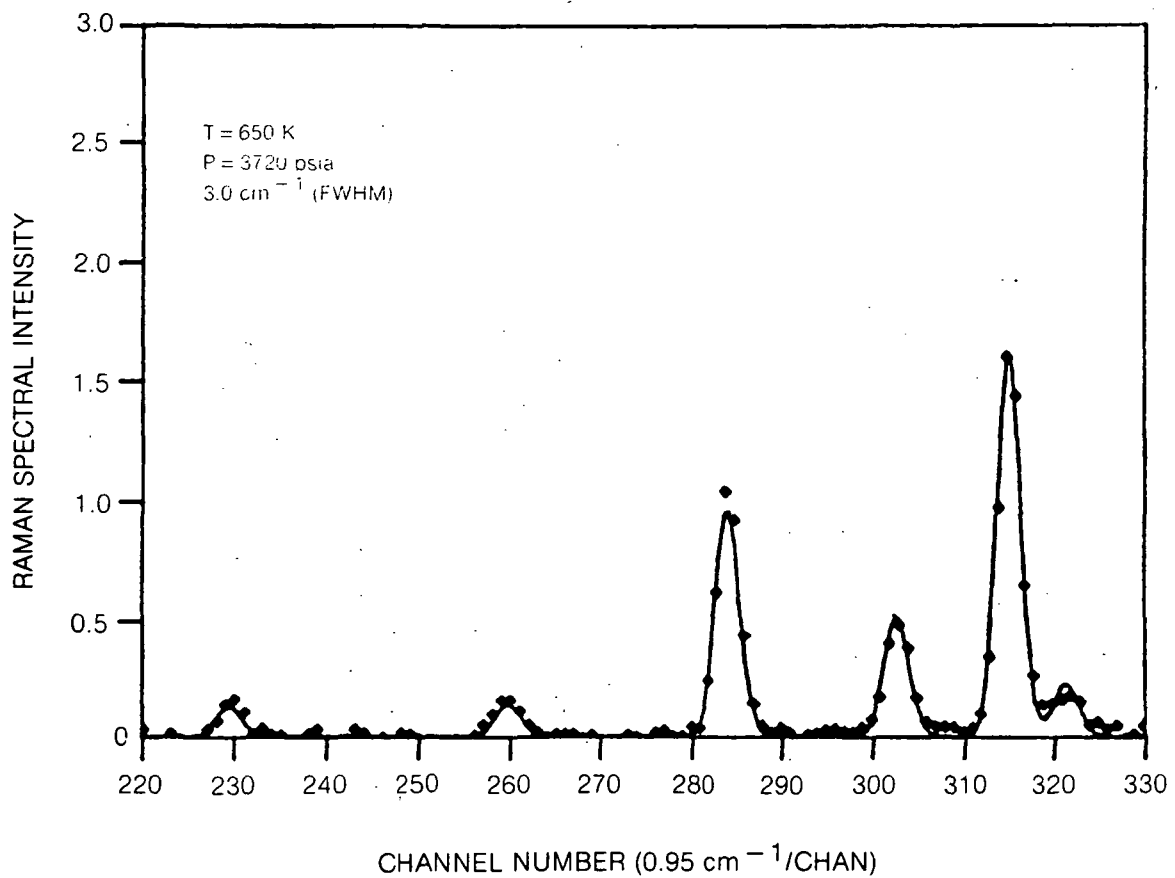
The spectrum at a moderate cell temperature, 650K, is shown in Fig. 14. The recorded temperature is the temperature of a tungsten-5% rhenium/tungsten-26% rhenium thermocouple inserted into the center of the cell under the heater element. Again the agreement with the calculations is good.

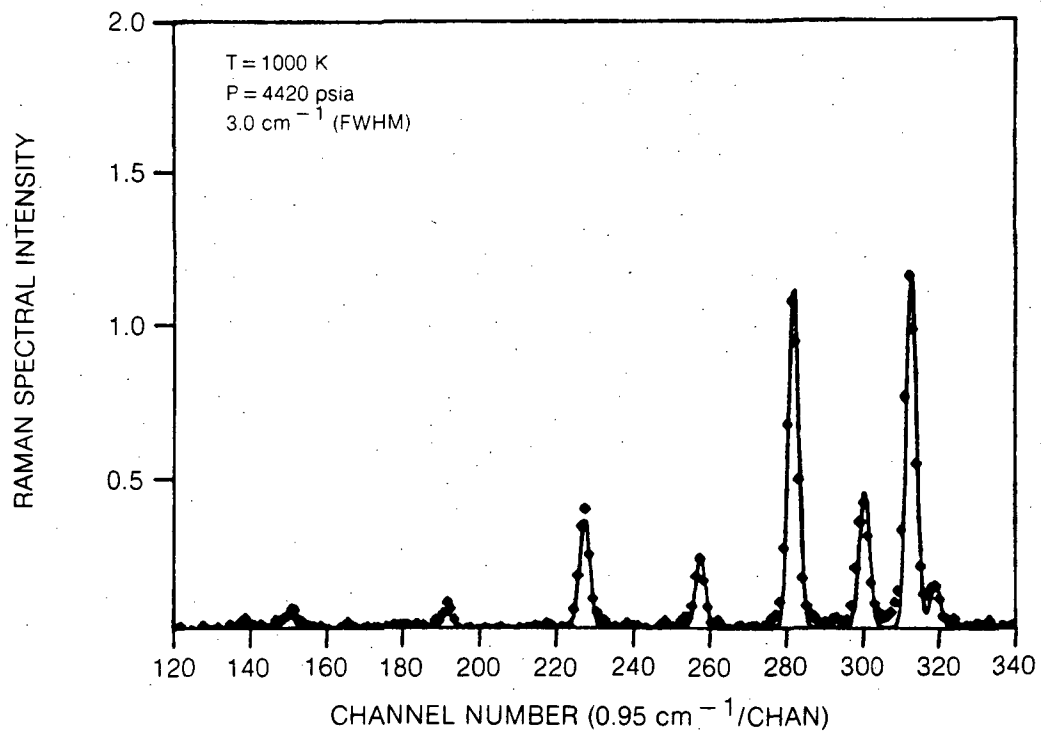
The Q-branch spectrum obtained with an indicated cell temperature of 1000K is shown in Fig. 15. The pressure in this case (4420 psia) is near the expected full scale hydrogen pressure. The nominal operating pressure in the fuel preburner is 5500 psia and the hydrogen mole fraction is about 0.89, therefore the hydrogen partial pressure is approximately 4900 psia. The final pressure in the heated cell is determined by the initial pressure and the

HYDROGEN Q-BRANCH RAMAN SPECTRUM



HYDROGEN Q-BRANCH RAMAN SPECTRUM



HYDROGEN Q-BRANCH RAMAN SPECTRUM

temperature rise after the cell is sealed off before heating. The final cell pressure is determined empirically, due to heat losses discussed previously. The agreement with calculations is very good.

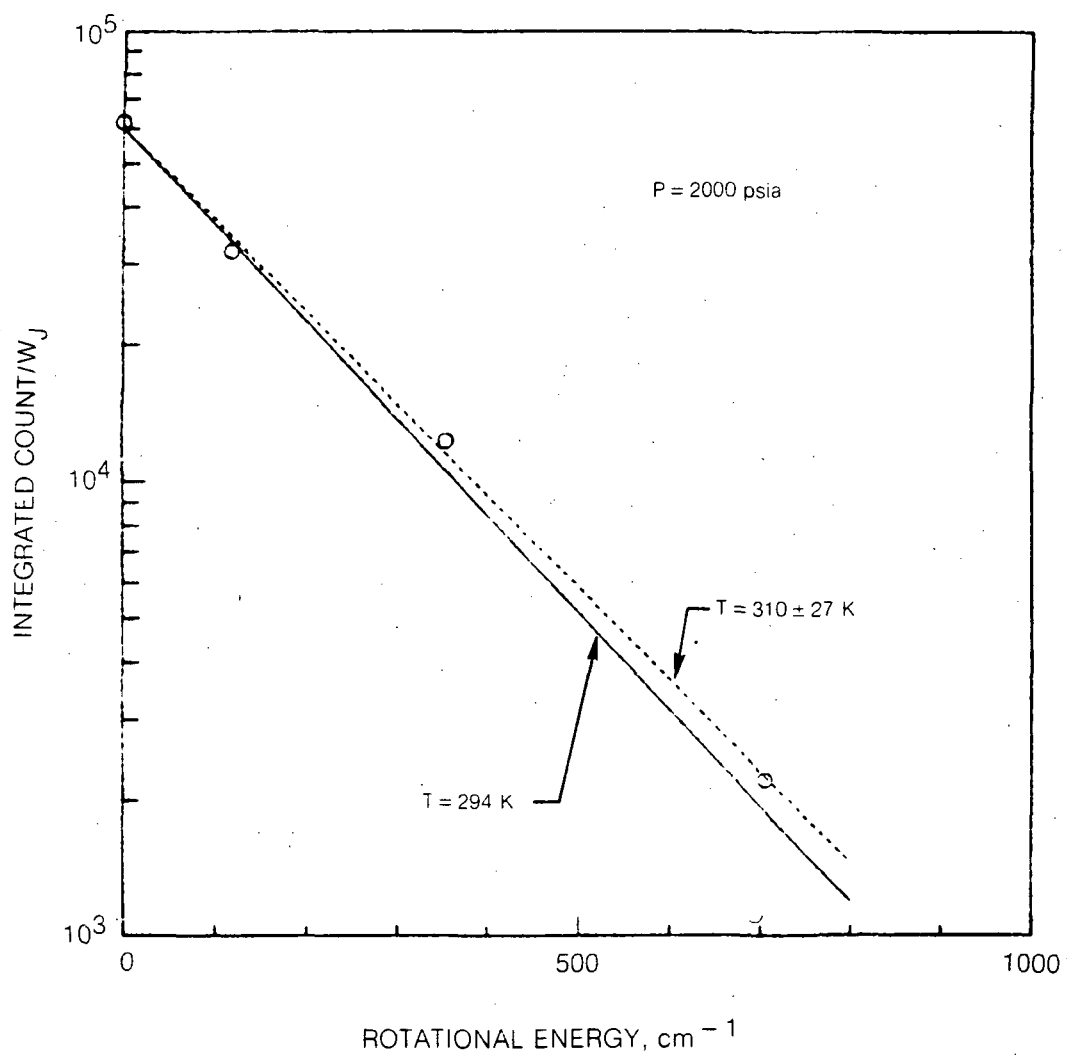
The vibrational Raman spectra have been analyzed to determine the temperature from the distribution of intensities. Representative results are shown in Figures 16, 17 and 18. The measured Q-branch transitions are integrated across the individual lines and normalized by the weighting factor, w_J and the system spectral responsivity. The weighting factor can be derived from Equation (14) of Reference 1 by rewriting the vibrational population as a Boltzmann factor times a function of J , the rotational quantum number. The weighting factor then is just the remaining function of J . The figures show as a solid line the dependence for the measured cell temperature. The dotted curve is a line least-squares fit to the experimental data. The temperature uncertainties reflect the uncertainty in the fit to the line (Ref. 8) and are seen to be less than 10 percent at the signal rates of these experiments.

Vibrational Raman spectra of hydrogen have been measured at a number of different combinations of temperature and pressure with the fiber optic system. The results of data reduction of a series of measurements with an indicated cell temperature of 1000 K are summarized in Table 2. The cell pressure in this series is 4420 psia. The temperature uncertainties determined from the quality of the least squares fit to the spectra are shown as well. It may be argued from this data that the temperature uncertainty overestimates the errors, although more data would be needed to definitively examine this point. It should be noted that, at present, the least squares analysis weights all the transitions equally. The proportional uncertainty of the high J transitions is greater, however so they are weighted perhaps too heavily. This aspect of the data reduction should be examined more closely in future investigations. There are other approaches to the data reduction, such as fitting the data point by point to spectra calculated with the known system spectral response. This method probably is slower, but perhaps not significantly depending on the computational power available.

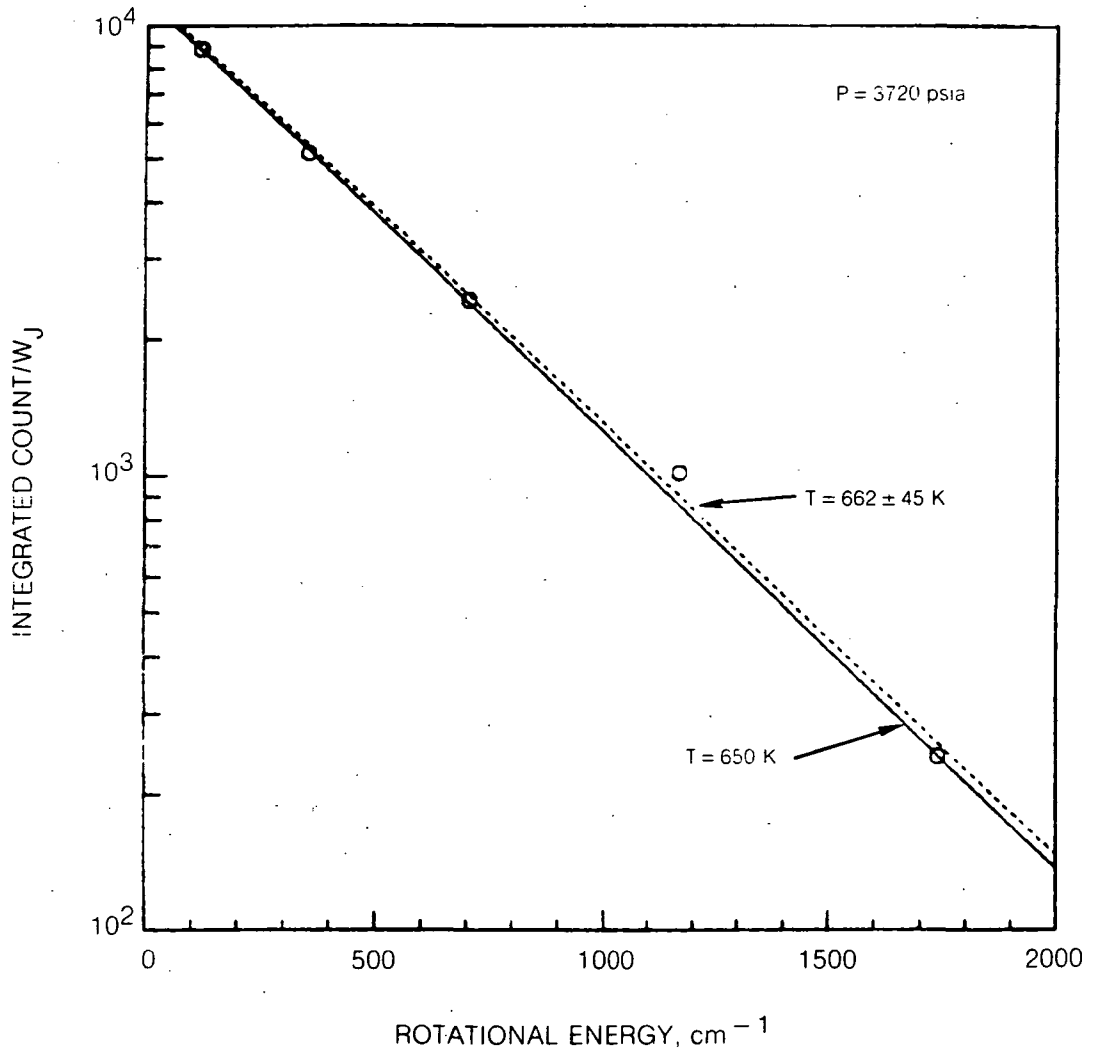
Comparison to Predicted Signal Rates

The measured signal rates were compared to predicted signal rates to assess the overall performance of the system and identify any problem areas. To do this the absolute spectral response of the optical system was measured.

A tungsten strip filament lamp was placed at the focal point in the probe volume. All system elements were the same with the exception that the cell window was not used. The effect of this window should be negligible. The lamp was heated to a relatively low temperature to avoid saturating the opti-

H₂ RAMAN TEMPERATURE ANALYSIS

H₂ RAMAN TEMPERATURE ANALYSIS



H₂ RAMAN TEMPERATURE ANALYSIS

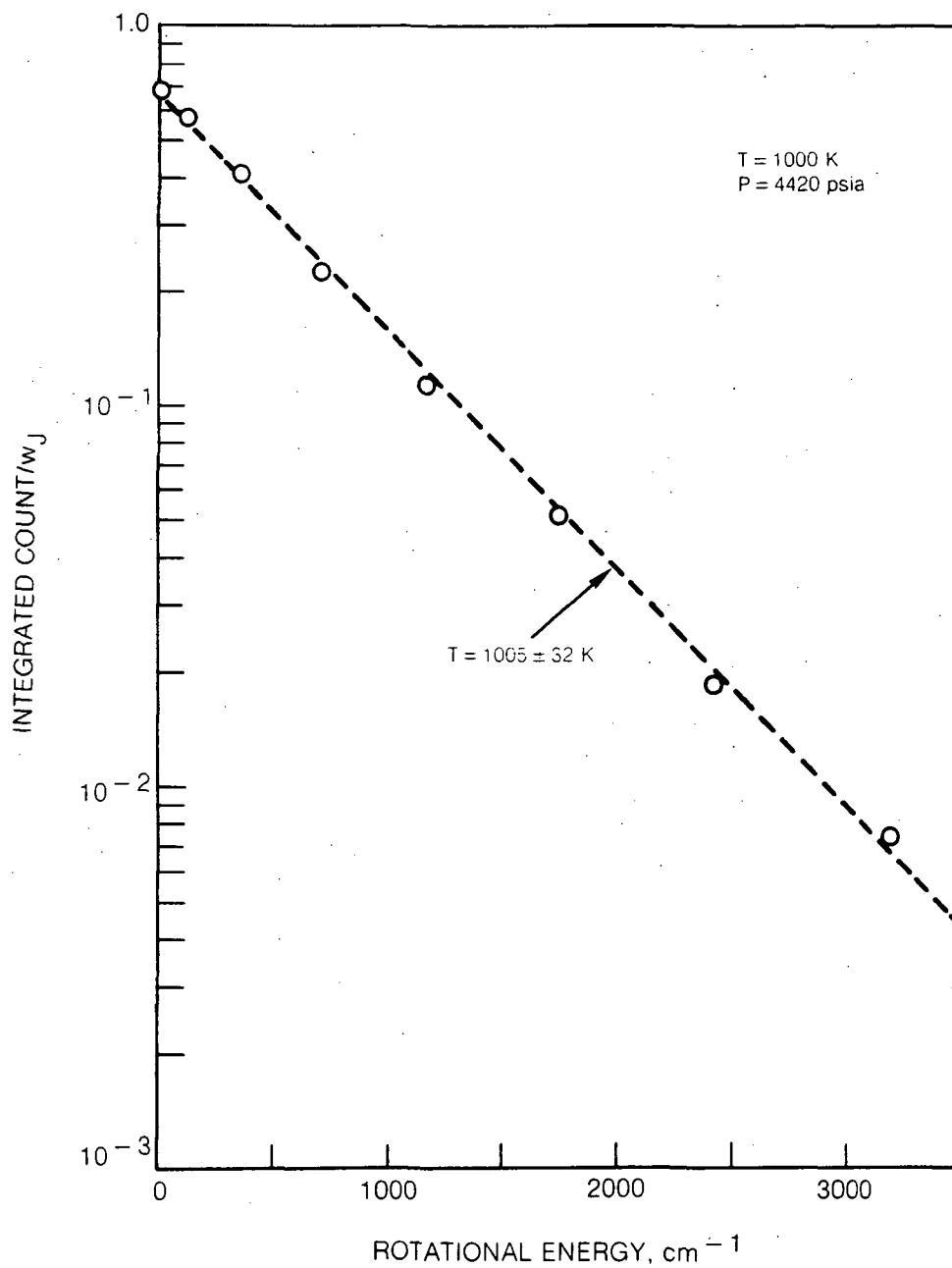


Table 2

Results of Raman Measurements at 1000K Cell Temperature

<u>Run</u>	<u>Measured Temperature, K</u>	<u>Temperature Uncertainty, K</u>
1	1005	32
2	1005	69
3	1047	66
4	1020	78
5	1021	111
6	1085	86
7	1179	133
8	840	86
9	925	51

cal multichannel detector. The lamp temperature, measured with a disappearing filament pyrometer, was 1540 K. The spectral intensity of the lamp was calculated from the analytic expressions of Pon and Hessler (Ref. 9) for the emissivity of tungsten as a function of temperature and wavelength. This calibration gives the overall system responsivity and includes: Fresnel reflection losses at all uncoated optical surfaces, transmission of the absorptive glass filter, geometrical blockage by the obscuration of the laser turning prism, transmission through the receiver fiber, grating efficiency, losses due to overfilling the spectrograph and the response of the optical multichannel detector. These factors correspond to the factors η_Q and ϵ_c of equation 30 in Reference 1. The measured system response is 4.1×10^{-4} counts/photon. If this is compared to estimates of the above factors, it is indicated that the grating is overfilled by a factor of 4.2, which corresponds to the beam expanding at $f/3.3$ into the $f/6.7$ spectrometer as it leaves the receiver fiber. This is very reasonable.

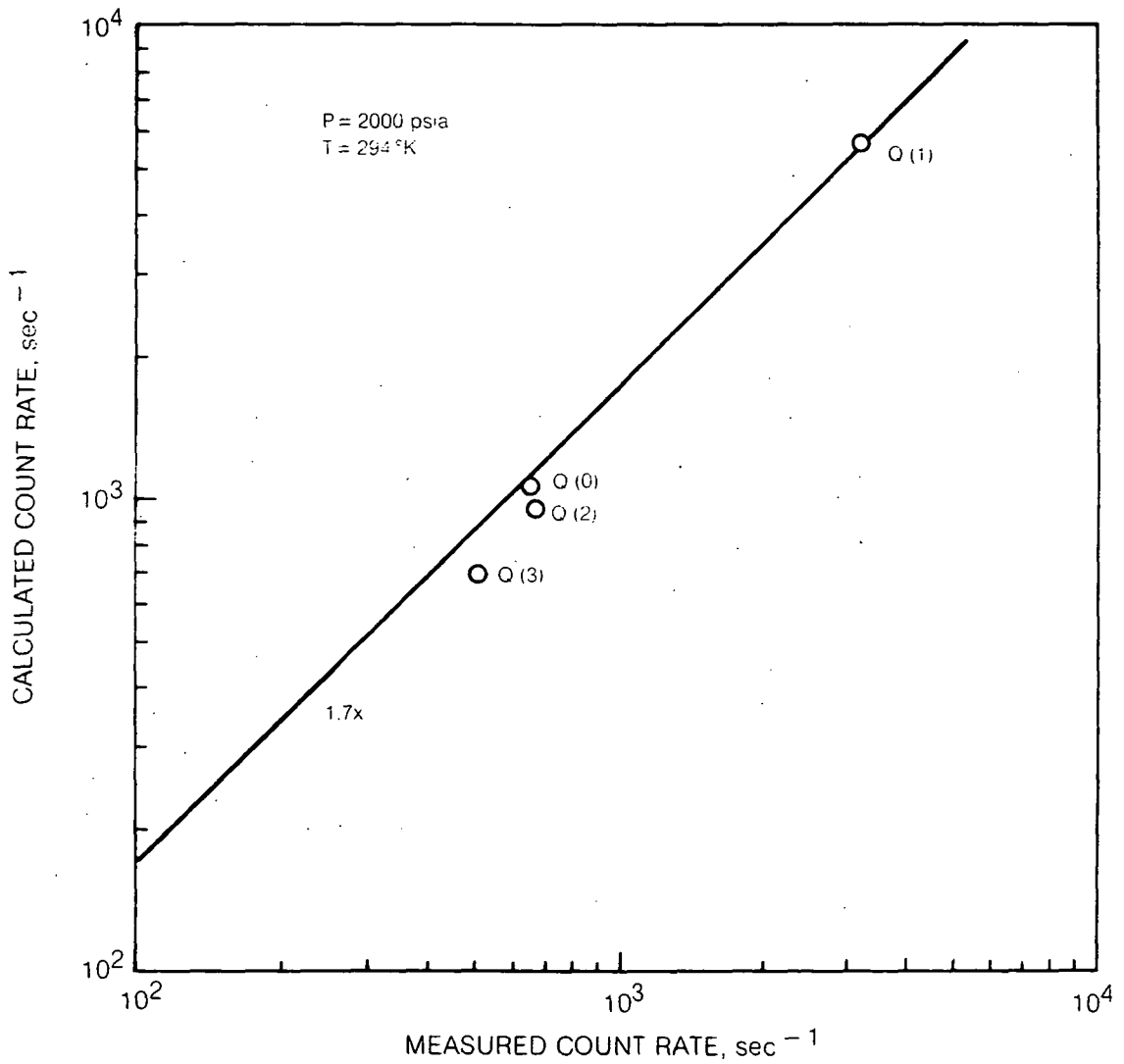
To compare predicted signal estimates with the measured Raman signal rates, the laser power and the spatial resolution were measured and the collection solid angle was estimated. The spatial resolution was determined by translating a 2 mm thick dye cell through the focal volume and observing the signal on the optical multichannel detector. The resolution measured was 1 cm and was less than measured previously as described in the section on the optical head. This possibly may be due to greater chromatic aberration effects in the former measurements, which should not affect the OMD measurements because the signal is dispersed. Another possible reason for the improved spatial resolution is that a higher quality lens was used in the Raman tests, leading to sharper focusing. The collection solid angle was estimated from the geometrical aperture of the the high pressure cell window, knowing the location of the focal point in the cell. The incident laser power was 0.5 Watts. More will be said about the incident laser power level in the discussion of the results.

The Raman spectrum measured at room temperature and 2000 psia is compared to the signal count rates calculated from the above system parameters in Figure 19. The measured signal count rates are integrated across the individual Q-branch components. The line fit to the data indicates that the two agree within a factor of 1.7. This is considered to be quite good. The only factor that has not been explicitly considered is that due to not focusing the collected Raman shifted radiation completely into the acceptance region of the receiver fiber. This is not accounted for in the spectral lamp calibration because the image of the filament overfills the fiber.

Discussion of Results

The laser transmission is not as high for the Raman tests as the 45 percent transmission measured in the fiber transmission tests and shown in

COMPARISON OF CALCULATED AND MEASURED COUNT RATES



Figures 2 and 3. In those measurements the focusing was adjusted to obtain maximum transmission through the fiber. Careful adjustment of the focus was found to be necessary in later tests to obtain the smallest spot size at the probe volume, however. This results in the laser radiation propagating in the lowest order modes in the fiber. With the microscope objective used for the Raman tests, the laser beam is focused to approximately 19 microns at the entrance to the fiber. With an incident power of 3.3 Watts, which was the maximum available from the medium frame laser used, the intensity is 1.2 MW/cm^2 . In Reference 1 the critical intensity for nonlinear conversion processes was estimated to be about 40 kW/cm^2 per transverse mode. Evidence for stimulated Raman scattering is shown in Figure 10. The threshold for stimulated Brillouin scattering is known to be lower than for Raman scattering, so Brillouin scattering is expected to affect the fiber transmission as well. Brillouin scattering occurs in the backward direction and requires special equipment to observe. The low transmission through the fiber when it is adjusted to produce the lowest order modes should not be surprising. Focusing into the fiber was adjusted while viewing the dye fluorescence signal. An optimum was found close to the condition giving low order fiber propagation modes. This suggests that it is necessary to have a small laser spot size to couple efficiently into the receiver fiber. Modes that do not focus well, overflow the receiver fiber entrance and are not collected.

The results of the measurements can be extended to reassess the performance of a fully developed optical system for measurements with a higher power laser and a spectrograph more closely matched to the receiver fiber. If a faster spectrograph and an intensified diode array are used, a collection efficiency of .066 and a detector response of .07 counts/photon is expected. This is a factor of 11 higher collection efficiency than obtained here. Taking the usable laser power as 2 Watts and the collection solid angle of .003 steradians, along with the design objectives of 0.01 second temporal resolution and, 1 cm spatial resolution, the average Raman signal count per transition is calculated to be 430 photons collected. This is expected to result in a temperature uncertainty of 70 K or 7 percent at 1000 K. If the optical speed of the system is increased to make more precise temperature measurements, then the f-number must be decreased to about f/5.7 to get a 25 K temperature precision. This modification should be considered for the test bed engine hardware.

The measurements and calculations are summarized in Table 3. The first two columns compare the measurements and calculations of Figure 19. The last two columns compare the predictions from the conceptual design report and the currently projected performance. The measurements represent a 30 second average. The combination of the collection and quantum efficiencies are the result of the tungsten lamp calibration. The total count represents the total

Table 3
Comparison of Raman Signal Estimates

<u>Quantity</u>	<u>Present Results</u>		<u>Est. Performance</u>	
	<u>Measured</u>	<u>Calculation</u>	<u>Ref. 1</u>	<u>Projection</u>
P_L , W	0.5	0.5	4	2
ϵ_c	} 0.0004	} 0.0004	0.2	0.066
η_q			0.2	0.07
Ω , sR	0.003	0.003	0.002	0.003
k_s , cm^{-1}	16322	16322	19600	16322
l , cm	1	1	1	1
t , sec	30	30	.01	.01
I_R , $\text{cm}^{-1} \text{sR}^{-1}$	-----	3(-9)*	5(-10)	3(-10)
N , counts	96k	167k	2500	430

*Refers to Q(1) line at 300 K and 2000 psia. The other Raman strengths correspond to an average transition at 1000 K and 5500 psia.

for the strongest Q(1) transition. The results in the first columns fall within the factor of 1.7 of each other as in Fig. 19. The projections from the conceptual design report are summarized in the third column, while the current projections of performance are shown in the last column. It should be noted that the projections in Reference 1 were for rotational Raman scattering, while the rest are for vibrational Q-branch scattering. The laser power, incident on the focal volume, has been scaled down, in recognition of the limited fiber transmission of modes which can be tightly focused. The quantum efficiency of the multichannel detector has been reduced because of the fall off of the detector efficiency in the red portion of the spectrum. An omission in the conceptual design report has been corrected. Optical multichannel detector efficiency is defined such that two detected photoelectrons are required for each registered count. The collection efficiency has been decreased by the obscuration factor which was neglected in the conceptual design reported, as stated therein. The Raman intensity I_R in the conceptual design was for one of the weaker transitions, while the projection in the last column is for an average transition.

CONCLUSIONS AND RECOMMENDATIONS

The feasibility of measuring temperature profiles in the SSME preburner has been investigated experimentally. The gas conditions existing in the preburner have been simulated by high pressure hydrogen contained in a heated optical cell. Experimental measurements have been made with available equipment, which, with care, can be extended to predict performance of a system designed for actual diagnostics. In particular the system can be scaled to higher laser power, a larger spectrometer aperture and a more sensitive detector.

One of the conclusions of this study is that attenuation of low order spatial modes in the optical fiber limits the laser intensity that can be realized at the laser focal spot in the probe volume. The probe volume is determined ultimately by the volume that can be coupled into the receiver fiber. Nonlinear scattering processes are probably responsible for the high attenuation of low order spatial modes.

The spatial resolution objective of 1 cm appears to be achievable at working distances of 100 to 300 mm, with collection solid angles of .003 steradians (not accounting for blockage).

It appears that a 5 % temperature resolution is feasible, keeping the original spatial and temporal resolution goals of 1 cm and 10 milliseconds. If a larger optical aperture can be provided, improved precision may be possible. Other trade-offs are possible. If the temporal resolution is relaxed to 0.1 sec, temperature precision close to 1 percent should be achievable.

It is recommended that a larger optical window be sought ($f/6$) and that it be located in the preburner as near the turbine entrance as practical. Placement of the laser close to the engine in an acoustic enclosure with suitable cooling provided is recommended. This is to minimize the length of the transmitter fiber. The design of the optical head should be considered in detail to ensure that spherical aberration and chromatic aberration do not limit working at the larger optical apertures. Finally it is recommended that a design objective of 5 percent temperature precision be considered for applications where high temporal response is desired.

REFERENCES

1. J. A. Shirley: Investigation of the Feasibility of Temperature Profiling Optical Diagnostics in the SSME Fuel Preburner. Final Technical Report prepared under NASA/Marshall Contract NAS8-34774, 1983.
2. R. G. Smith: "Optical Power Handling Capacity of Low Loss Optical Fibers as Determined by Stimulated Raman and Brillouin Scattering." Appl. Optics, Vol. 11, pp. 2409-2494, 1972.
3. Y. Susaki and A. Tachibana: "Measurement of the μm Sized Radius of Gaussian Laser Beam Using the Scanning Knife-Blade Technique." Appl. Optics Vol. 14, pp. 2809-2810, 1975.
4. A. C. Eckbreth and J. W. Davis: "Spatial Resolution Enhancement in Coaxial Light Scattering Geometries." Appl. Optics, Vol. 16, pp. 804-806, 1977.
5. W. D. Johnston, Jr., I. P. Kaminov and J. G. Bergman, Jr.: "Stimulated Raman Gain Coefficient for LiNbO_3 , $\text{Ba}_2\text{NaNb}_5\text{O}_{15}$, and Other Materials." Appl. Phys. Lett., Vol. 13, pp. 190-193, 1968.
6. R. R. Rudder and D. R. Bach: "Rayleigh Scattering of Ruby-Laser Light by Neutral Gases." J. Opt. Soc. Amer., Vol. 58, pp. 1260-1266, 1968.
7. R. O. Kagel: "Raman Spectroscopy" in Handbook of Spectroscopy, Vol. II, J. W. Robinson, Ed., CRC Press, 1974, p. 111.
8. E. D. Crow, F. A. Davis and M. W. Maxfield: Statistics Manual. Dover, New York, 1960, p. 160.
9. R. M. Pon and J. P. Hessler: "Spectral Emissivity of Tungsten: Analytic Expressions for the 340-nm to 2.6- μm Spectral Region." Appl. Optics, Vol. 23, pp. 975-976, 1984.

REPORT DOCUMENTATION PAGE

1a. REPORT SECURITY CLASSIFICATION None		1b. RESTRICTIVE MARKINGS None	
2a. SECURITY CLASSIFICATION AUTHORITY		3. DISTRIBUTION / AVAILABILITY OF REPORT	
2b. DECLASSIFICATION / DOWNGRADING SCHEDULE			
4. PERFORMING ORGANIZATION REPORT NUMBER(S) R85-956642		5. MONITORING ORGANIZATION REPORT NUMBER(S)	
6a. NAME OF PERFORMING ORGANIZATION United Technologies Research Center	6b. OFFICE SYMBOL (if applicable) UTRC	7a. NAME OF MONITORING ORGANIZATION George C. Marshall Space Flight Center Marshall Space Flight Center	
6c. ADDRESS (City, State, and ZIP Code) East Hartford, Connecticut 06108		7b. ADDRESS (City, State, and ZIP Code) Huntsville, Alabama 35812	
8a. NAME OF FUNDING / SPONSORING ORGANIZATION George C. Marshall Space Flight Center	8b. OFFICE SYMBOL (if applicable)	9. PROCUREMENT INSTRUMENT IDENTIFICATION NUMBER NAS8-34655	
8c. ADDRESS (City, State, and ZIP Code) Huntsville, Alabama 35812		10. SOURCE OF FUNDING NUMBERS	
		PROGRAM ELEMENT NO.	PROJECT NO.
		TASK NO.	WORK UNIT ACCESSION NO.
11. TITLE (Include Security Classification) Investigation of Breadboard Temperature Profiling System for SSME Fuel Preburner Diagnostics			
12. PERSONAL AUTHOR(S) Shirley, John Allen			
13a. TYPE OF REPORT Final Technical	13b. TIME COVERED FROM 10/83 TO 5/85	14. DATE OF REPORT (Year, Month, Day) 1986, January, 17	15. PAGE COUNT 39
16. SUPPLEMENTARY NOTATION			
17. COSATI CODES		18. SUBJECT TERMS (Continue on reverse if necessary and identify by block number)	
FIELD	GROUP	RAMAN OPTICAL FIBER	
		HYDROGEN	
		LASER SPECTROSCOPY	
19. ABSTRACT (Continue on reverse if necessary and identify by block number) The feasibility of measuring temperatures in the space shuttle main engine (SSME) fuel preburner using spontaneous Raman scattering from molecular hydrogen has been studied experimentally. Laser radiation is transmitted to the preburner through a multimode optical fiber. Backscattered Raman-shifted light is collected and focused into a second fiber which connects to a remotely-located spectrograph and a multichannel optical detector. Optics collimate and focus laser light from the transmitter fiber defining the probe volume, which is approximated by a cylinder 8 mm long, and 0.3 mm in diameter. The high pressure (5500 psia), high temperature (1000K) preburner environment has been simulated by a heated pressure cell having windows and containing pure hydrogen. Temperatures determined by the distribution of Q-branch ro-vibrational transitions demonstrate precision and accuracy of 3 percent. The measurements indicate that preburner temperatures can be determined with 5 percent accuracy with spatial resolution less than 1 cm and temporal resolution of 10 milliseconds at the nominal preburner operating conditions.			
20. DISTRIBUTION / AVAILABILITY OF ABSTRACT <input type="checkbox"/> UNCLASSIFIED/UNLIMITED <input type="checkbox"/> SAME AS RPT. <input type="checkbox"/> DTIC USERS		21. ABSTRACT SECURITY CLASSIFICATION UNCLASSIFIED	
22a. NAME OF RESPONSIBLE INDIVIDUAL		22b. TELEPHONE (include Area Code)	22c. OFFICE SYMBOL